Showcasing research from Professor Yang Song's laboratory, State Key Laboratory of Environmental Chemistry and Ecotoxicology, Research Center for Eco-Environmental Sciences, Chinese Academy of Sciences, Region, Country.

Copper oxide nanoparticles induce cuproptosis and ferroptosis through mitochondrial concatenation

This work demonstrates that cuproptosis and ferroptosis can be interconnected via mitochondria. Specifically, exposure to CuO NPs leads to cuproptosis in RAW264.7 cells through the accumulation of copper ions. Cuproptosis leads to the inhibition of mitochondrial membrane lipid synthesis, resulting in mitochondrial damage and disruption of intracellular redox balance, ultimately leading to ferroptosis. In vivo, both cuproptosis and ferroptosis were found to contribute to liver damage caused by CuO NPs, along with reduced lipid levels, mitochondrial impairment, and redox imbalance. Copyright owner: Muran Jiang.

As featured in:

See Xiaoqi Tao, Yang Song *et al.*, *Environ. Sci.: Nano*, 2024, **11**, 4089.

ROYAL SOCIETY
OF **CHEMISTRY**

rsc.li/es-nano

PAPER

Check for updates

Copper oxide nanoparticles induce cuproptosis and ferroptosis through mitochondrial concatenation†

Muran Jiang,[a] Xiaoqi Tao,*[ab] Yingxin Pang,[a] Zongmin Qin,[a] Erqun Song [iD][c] and Yang Song [iD]*[d]

Copper oxide nanoparticles (CuO NPs) will accumulate in soil and water due to human and natural activities, eventually finding their way into the human body through direct or indirect pathways. Therefore, it is crucial to study the biosafety of CuO NPs. CuO NPs primarily damage cells through CuO particles and copper ions, with intracellular copper ion overload being a critical factor in cuproptosis. However, the potential of CuO NPs to trigger cell cuproptosis has not been thoroughly investigated. While some studies have explored the relationship between cuproptosis and ferroptosis, the precise mechanism connecting the two remains unclear. Here, we have discovered that exposure to CuO NPs triggers cuproptosis in RAW264.7 cells. This process leads to the inhibition of mitochondrial membrane lipid synthesis, resulting in mitochondrial damage and disruption of intracellular redox balance, ultimately leading to ferroptosis. *In vivo*, both cuproptosis and ferroptosis were found to contribute to liver damage caused by CuO NPs, along with reduced lipid levels, mitochondrial impairment, and redox imbalance. In summary, our research contributes to the assessment of the biocompatibility of CuO NPs and offers additional insights into the mechanisms underlying cuproptosis.

Environmental significance

Research estimates that approximately 200 metric tons of Cu NPs and CuO NPs were manufactured in 2010, with 36 tons being deposited in soil and 11 tons in water. The accumulation of CuO NPs in environment, compounded by the bioaccumulation effect within the food chain, might ultimately result in elevated human exposure to concentrated CuO NPs. Furthermore, CuO NPs are extensively employed in multiple fields due to outstanding performance, which heightens the potential for worker exposure to CuO NPs. Research on the toxicity of CuO NPs is highly important due to their ability to enter the human body through both direct (respiration, ingestion) and indirect (food chain accumulation) routes. Interaction with CuO NPs may result in immune toxicity, reproductive toxicity, neurotoxicity, inflammation, and other adverse effects, which collectively indicate the potential toxicity of CuO NPs to humans. Our study involved exposing RAW264.7 cells and C57BL/6 mice to CuO NPs, revealing CuO NPs led to liver damage through cuproptosis and its mediation of ferroptosis.

[a] *Key Laboratory of Luminescence Analysis and Molecular Sensing, Ministry of Education, College of Food Science, Southwest University, 2 Tiansheng Rd, Beibei District, Chongqing, 400715, China. E-mail: taoxiaoqi@swu.edu.cn*
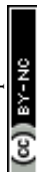
[b] *Joint International Research Laboratory of Animal Health and Animal Food Safety, College of Veterinary Medicine, Southwest University, 2 Tiansheng Rd, Beibei District, Chongqing, 400715, China*

[c] *Key Laboratory of Luminescence Analysis and Molecular Sensing, Ministry of Education, College of Pharmaceutical Sciences, Southwest University, 2 Tiansheng Rd, Beibei District, Chongqing, 400715, China*

[d] *State Key Laboratory of Environmental Chemistry and Ecotoxicology, Research Center for Eco-Environmental Sciences, Chinese Academy of Sciences, 18 Shuangqing Rd, Haidian District, Beijing, 100085, China.*
E-mail: yangsong@rcees.ac.cn

† Electronic supplementary information (ESI) available. See DOI: **https://doi.org/10.1039/d4en00455h**

1. Introduction

Metal oxide nanoparticles are extensively applied, due to their common nanoscale dimensions and high surface area ratio of metal. Simultaneously, distinctions in the physical and chemical properties among various metal oxide nanoparticles result in divergent application domains.[1,2] Among these, copper oxide nanoparticles (CuO NPs) are prominently featured in sectors such as sensor technology,[3] food packaging,[4] nano-delivery systems,[5] and agricultural fungicides,[6] owing to their exceptional reactivity, chemical stability, oxidizing characteristics, and antibacterial properties.[7] CuO NPs can enter the environment through human and natural activities,[8,9] accumulating in water and soil,[10] and eventually making their way into the human body through direct[11,12] (respiration,

This journal is © The Royal Society of Chemistry 2024

Environ. Sci.: Nano, 2024, **11**, 4089–4101 | **4089**

ingestion) or indirect[9] (food chain accumulation) routes. Consequently, investigating the biosafety of CuO NPs is of paramount importance. Previous studies have demonstrated that exposure to CuO NPs can trigger oxidative stress, mitochondrial impairment, DNA damage, endoplasmic reticulum stress, cell cycle arrest and protein misfolding, culminating in apoptosis, necroptosis, pyroptosis, autophagy, ferroptosis and cuproptosis.[11–18] *In vivo*, CuO NPs exposure can result in immunotoxicity,[15] reproductive toxicity,[19] neurotoxicity,[20] organ necrosis[21] and developmental toxicity.[22]

Recently, a novel form of cell death, designated cuproptosis, has been identified. This form of cell death is contingent upon intracellular copper ion concentration.[23] Cuproptosis induces protein toxicity stress by promoting the aggregation of copper-induced lipoylated proteins and the loss of Fe–S cluster proteins.[23] Recent research has primarily focused on inducing cuproptosis for cancer treatment by directly increasing intracellular copper levels by constructing materials containing copper.[24–26] However, the influence of CuO NPs on cuproptosis and the precise mechanisms underlying cuproptosis, including its specific impact on cell death and its relationship with other forms of cell death, remain incompletely understood.[27]

Apart from its role in cuproptosis, copper also plays a regulatory role in maintaining intracellular iron balance through diverse mechanisms, consequently influencing ferroptosis.[28–30] Ferroptosis, reliant on iron, commonly exhibits the alteration of mitochondrial morphology and the disturbance in intracellular redox equilibrium.[31] The initiation of ferroptosis can be facilitated by various mechanisms, including adjustments in intracellular glutathione (GSH) levels, iron equilibrium, polyunsaturated fatty acid (PUFA) content, and glutathione peroxidase 4 (GPX4) activity.[31] Additionally, recent research suggests that GSH is involved in both cuproptosis and ferroptosis processes.[32] Erastin, the ferroptosis activator, can induce cuproptosis by suppressing FDX1 protein degradation.[33] Furthermore, copper ions can directly combine with GPX4, facilitating the ubiquitination and aggregation of GPX4, ultimately leading to ferroptosis.[34] While these studies demonstrate a correlation between cuproptosis and ferroptosis, the mechanistic link between these two forms of cell death has yet to be fully elucidated.

In order to clarify the influence of cuproptosis on the biocompatibility of CuO NPs and delve deeper into the mechanical interplay between cuproptosis and ferroptosis, we exposed RAW264.7 cells to CuO NPs with or without inhibitors and mimicked human exposure to CuO NPs through oral gavage in mice. The current finding demonstrates that cuproptosis serves as a key toxic mechanism of CuO NPs, damaging mitochondria to induce ferroptosis by disrupting mitochondrial membrane lipid synthesis.

2. Materials and methods

2.1 Materials

CuO NPs (<200 nm) were obtained from Macklin (Shanghai, China). *N*-Acetyl cysteine (NAC), tetrathiomolybdate (TTM), 2′,7′-dichlorodihydrofluorescein diacetate (DCFH-DA) and BODIPY 581/591 C11 (C11-BODIPY) were purchased from Sigma-Aldrich Co. (St Louis, MO, USA). Erastin was bought from Yuanye Biotechnology (Shanghai, China). RIPA lysis buffer was obtained from Beyotime Institute of Biotechnology (Nanjing, China). Bicinchoninic acid (BCA) assay kit was purchased from Dingguo Biotechnology Co., Ltd. (Beijing, China). High ECL Enhanced Western Blotting Substrate was purchased from BIOGROUND (Chongqing, China). The total RNA extraction reagent was purchased from Tiangen Biochemical Technology Co., Ltd (Beijing, China). MitoSOX Red mitochondrial superoxide indicator, cell counting kit 8 (CCK8), JC-1 mitochondrial membrane potential (MMP) assay kit, integrated cDNA synthesis SuperMix and 2× SYBR Green qPCR Mix were provided by Yeasen Biotechnology Co., Ltd (Shanghai, China). Phosphate buffer saline (PBS) and hematoxylin–eosin (H&E) staining dyes were purchased from Servicebio Biotechnology Co (Wuhan, China). 4,6-Diamidino-2-phenylindole (DAPI) was purchased from Wanlei Biotechnology Co., Ltd. (Shenyang, China). Adenosine triphosphate (ATP) kit was bought from Solarbio Science & Technology Co., Ltd (Beijing, China). Malondialdehyde (MDA), GSH, pyruvic acid (PA), total cholesterol (T-CHO), triglycerides (TG), superoxide dismutase (SOD), aspartate aminotransferase (AST), and alanine aminotransferase (ALT) kits were provided from Nanjing Jiancheng Bioengineering Institute (Nanjing, China). GPX4 and lipoylsynthase (LIAS) primary polyclonal antibodies and Mito-TEMPO were supplied by Santa Cruz Biotechnology (Santa Cruz, California, USA). Dulbecco's modified Eagle's medium (DMEM), fetal bovine serum (FBS), real-time quantitative polymerase chain reaction (RT-qPCR) amplification primers, β-actin primary monoclonal antibody, goat anti-rabbit IgG-HRP conjugated secondary and antibody, goat anti-mouse IgG-HRP conjugated secondary antibody were synthesized by Sangon Biotech Co., Ltd (Shanghai, China).

2.2 Characterization of CuO NPs

Based on the manufacturer's instructions, the particle size of CuO NPs ranges from 100–200 nm. To confirm the physicochemical characteristics of CuO NPs, CuO NPs were dissolved and diluted to 20 μg mL^{-1} and dispersed by ultrasonic dispersion for 10 min. 10 μL of the solution was dropped on the copper grid, air-dried at room temperature, and then the size and morphology of CuO NPs were observed using 120 kV transmission electron microscopy (TEM, Hitachi HT7800). Additionally, CuO NPs captured by TEM were quantitatively analyzed using Nano Measurer version 1.2.5 and fitted to Gaussian curves in OriginPro 2021 version 9.8.0.200. To detect changes in the physical properties of CuO NPs when subjected to different dispersion solutions, CuO NPs were diluted to 2 μg mL^{-1} in H$_2$O and DMEM, respectively. The hydrodynamic diameter and surface zeta potential charge of CuO NPs were assessed *via* dynamic light scattering (DLS) utilizing a Malvern Zetasizer Nano ZEN3700 (Malvern, Massachusetts, U.K.).

4090 | *Environ. Sci.: Nano*, 2024, **11**, 4089–4101

This journal is © The Royal Society of Chemistry 2024

2.3 Cell culture and treatment

Mouse leukemic monocyte–macrophage RAW264.7 cells were procured from Jiangsu KeyGEN Biotechnology Co. RAW264.7 cells were cultured in 5% CO_2 at 37 °C with DMEM complete medium containing 10% FBS, 100 U mL^{-1} penicillin, 100 mg L^{-1} streptomycin, 110 μg mL^{-1} sodium pyruvate, and 2 mM L-glutamine. RAW264.7 cells were cultured in vitro and seeded in either 96-well or 6-well plates for 24 h at a constant temperature. Following the incubation period, RAW264.7 cells were subjected to various concentrations of CuO NPs, 0, 5, 10, and 20 μg mL^{-1}, dissolved in DMEM medium without FBS for 12 h at cell densities ranging from 5×10^5 cells per mL to 1×10^6 cells per mL. For inhibition experiments, RAW264.7 cells were pre-treated with various inhibitors (100 μM TTM, 10 mM NAC, 10 μM erastin, 10 μM Mito-TEMPO) for 1 h before 20 μg mL^{-1} CuO NPs stimulation.

2.4 Cell viability

RAW264.7 cells were cultured by uniform inoculation into 96-well plates in 5% CO_2, 37 °C for 24 h at constant temperature. Subsequently, RAW264.7 cells were exposed to 20 μg mL^{-1} CuO NPs for 0, 3, 6, 12, and 24 h and various concentrations (0, 5, 10, 20 μg mL^{-1}) of CuO NPs for 12 h. After treatment, the cell culture medium was aspirated from the plates, and the wells were rinsed thrice with sterile PBS. Then, 100 μL of CCK8 solution, whose component was 100 μL serum-free DMEM medium with 10% (or 10 μL) of CCK8 reagent, was added to each well and incubated at 37 °C for 1 h. The absorbance at 450 nm was measured using a microplate reader (MD, SpectraMax iD3) to determine cell viability.

2.5 Copper and iron accumulation

RAW264.7 cells were evenly distributed into 6-well plates and exposed to different concentrations of CuO NPs solution for 12 h. The obtained precipitates were gathered through centrifugation at 100g for 5 min and then mixed with HNO_3 and H_2O_2 in a volumetric ratio of 3 : 1. This amalgam was then subjected to overnight incubation in a water bath set at 65 °C. The supernatant was finally diluted tenfold, and the intracellular copper and iron levels were determined using an Inductively Coupled Plasma Optical Emission Spectrometer (ICP-OES) (Avio 200, PerkinElmer, MA, USA). Each sample underwent analysis at least three times, and the outcomes were presented as the mean concentration in units of μg mL^{-1}. The elemental copper and iron contents in μg g^{-1} were determined in tissues, heart, liver, spleen, lung, kidney, brain, and testes, using the same method.

2.6 Reverse transcription real-time quantitative PCR assay (RT-qPCR)

Total RNA of RAW264.7 and liver tissue were extracted with TRNzol Universal total RNA extraction reagent following the manufacturer's instructions. The purified RNA (3 μg) was reverse transcribed into cDNA using a reverse transcription

kit. Subsequently, the relative expression levels of the target gene were determined using RT-qPCR with 2× SYBR Green qPCR master mix and an RT-qPCR detection system (Roche, Switzerland). The specific binding capacity of primers was utilized to measure the fluorescence expression difference (ΔCt) between the target gene and the reference gene, β-actin. Each experiment was conducted in triplicate. Primer sequences used in experiments are listed in Table S1.†

2.7 Western blotting (WB)

Utilizing RIPA lysis buffer for cell or tissue lysis in the ice bath for at least 30 min, the resulting mixture was then centrifuged at 10 000g, 4 °C for 10 min to collect the liquid above the sediment. Subsequently, the protein concentration was measured using a BCA assay kit as per the manufacturer's instructions. The remaining lysate was supplemented in 4 : 1 (v/v) ratio with 5× loading buffer and subjected to denaturation at 97 °C for about 10 min. Following denaturation, proteins (30 μg) were separated based on their molecular weights through SDS-PAGE analysis, transferred onto a nitrocellulose (NC) membrane, and the unbound sites were blocked with 5% BSA solution. The membrane was then probed with the respective primary antibody (1 : 2000) and secondary antibody (1 : 2000) for the target protein, and the protein signal was detected using high ECL enhanced Western blotting substrate. Finally, the grayscale values were quantified using Image J version 1.53c.

2.8 Flow cytometer analysis (FC)

RAW264.7 cells were harvested following centrifugation at 100g for 5 min, with or without inhibitor treatment of CuO NPs. Subsequently, the RAW264.7 cells were individually incubated with DCFH-DA (1 : 1000), C11-BODIPY (1 : 2000), MitoSOX (1 : 2000), and JC-1 MMP (1 : 1000) at 37 °C for 30 min. After a single wash with PBS, fluorescence intensity was assessed in various channels (FITC/PE) using a flow cytometer (FACS Melody, BD Biosciences, San Jose, CA, USA) to examine intracellular and mitochondrial ROS, lipid peroxidation (LPO), and alterations in mitochondrial membrane potential. The data obtained were subsequently analyzed and processed utilizing FlowJo version 10.8.1 (FlowJo LLC data analysis software, Ashland, OR, USA).

2.9 Animals and treatment

Male C57BL/6 mice, aged 6–8 weeks and obtained from Chongqing Traditional Chinese Medicine Research Institute, were kept in a controlled standard environment at 24 ± 2 °C with a 12 h light/dark cycle. All animal procedures were performed in accordance with the Guidelines for Care and Use of Laboratory Animals of Southwest University and approved by the Animal Ethics Committee of Southwest University Animal Care and Use Committee (approval number IACUC-20240428-01). Before the experiment, the mice underwent a week acclimatization period. Subsequently, those with unrestricted access to water and food were randomly assigned to three groups based on the gradient of gavage drug concentrations (0, 10 and 100 mg kg^{-1}), with

This journal is © The Royal Society of Chemistry 2024

Environ. Sci.: Nano, 2024, 11, 4089–4101 | 4091

three mice in each group. Gavage administration was performed once daily for 35 days, with the control group receiving physiological saline. Following the final gavage, the mice were subjected to 24 h fasting period, followed by anesthesia with isoflurane and euthanasia. Blood plasma and major organs, including the heart, liver, spleen, lungs, kidneys, brain, and testes, were assembled for evaluation. Part of the liver was fixed in 4% paraformaldehyde solution for frozen section preparation, and the remainder was stored at −80 °C.

2.10 Histopathological analysis

The liver, fixed with a 4% paraformaldehyde solution, underwent dehydration in 15% and 30% sucrose solutions for 24 h. Liver tissue slices, approximately 3 mm in thickness, were embedded in Sakura Tissue-Tek Compound (4583, USA) for cryopreservation. Subsequently, the embedded liver tissue was sectioned into 15 μm thick frozen slices employing a freezing microtome (CM1950, Leica, Wetzlar, Germany).

After allowing the frozen liver tissue sections to thaw to room temperature, they were immersed in a 4% paraformaldehyde solution for 15 min. Subsequently, staining was performed according to the instructions provided in the H&E staining kit, followed by air-drying and sealing with neutral resin. The prepared sections were then examined and imaged using an inverted fluorescence microscope (Olympus, IX71, Japan).

2.11 Fluorescent probe staining

After the frozen liver tissue sections were brought to room temperature, they were immersed in a 4% paraformaldehyde solution for 15 min. Subsequently, each sections of liver tissue were individually incubated at 37 °C for 1 h with DCFH-DA (1 : 200), C11-BODIPY (1 : 200), and JC-1 MMP (1 : 200). After being washed with PBS thrice, the slices were stained with DAPI solution at 37 °C for additional 10 min. Following PBS washing, the sections were sealed with neutral resin. The prepared slices were imaged using a laser scanning confocal microscope (LSCM, Nikon, Tokyo, Japan). The captured images were adjusted for fluorescence intensity using Viewer 5.21.00 (image processing software supplied with the LSCM, Nikon, Tokyo, Japan), and the fluorescence intensity of the adjusted images was quantified using Image J version 1.53c for further analysis of significant differences.

2.12 Biochemical analysis

After being exposed to CuO NPs for 12 h, with or without inhibitors, RAW264.7 cells were collected by centrifugation at 100g for 5 min. The collections were subjected to three freeze–thaw cycles and subsequently sonicated for 10 min to prepare cell homogenate for subsequent biochemical analysis.

A precise quantity of liver tissue was obtained, and physiological saline was added to the liver at a ratio of 1 : 9 (m/v). The liver tissue was mechanically disrupted in an ice bath to generate liver homogenate. Following this, the homogenate was centrifuged at 400g for 10 min, and the resulting supernatant was gathered for further biochemical analysis.

Biochemical components in RAW264.7 cells, plasma, and liver tissue were analyzed utilizing the corresponding reagent kits supplied by the Nanjing Institute of Biomedical Engineering Research, following the provided instructions. The components assessed included MDA, GSH, ATP, PA, T-CHO, TG, ALT, AST and SOD.

2.13 Statistical analysis

The data in each group were independently replicated at least three times, and all results were reported as mean ± standard deviation (SD). Group variances were evaluated for significance through one-way ANOVA combined with least significant difference (LSD) multiple comparison tests. A statistical significance threshold of $p < 0.05$ was applied. Graphs were generated using Prism GraphPad version 8.0.2 (GraphPad Software, Inc.).

3. Result

3.1 The physical properties characterization and cytotoxicity of CuO NPs

The physical properties of CuO NPs were characterized using a combination of TEM and DLS. The findings reveal that the shape of CuO NPs closely resembles a spherical shape, with sizes predominantly around 80 nm (Fig. 1A and B). When dispersed in ddH$_2$O, the average hydrodynamic size of CuO NPs measures 367.13 ± 25.44 nm, accompanied by a zeta potential of −13.96 ± 0.09 mV. In addition, dispersion in DMEM culture medium results in an average hydrodynamic size and zeta potential of 442.90 ± 21.01 nm and −7.01 ± 0.69 mV, respectively (Fig. 1C and D). RAW264.7 cells were exposed to 20 μg mL^{-1} CuO NPs for 0, 3, 6, 12, and 24 hours, and additionally to 0, 5, 10, and 20 μg mL^{-1} CuO NPs for 12 hours to assess the cytotoxicity of CuO NPs. As depicted in Fig. 1E and F, both time and dose-dependent impact of CuO NPs on RAW264.7 cells were observed. Additionally, in order to delve deeper into the mechanisms underlying CuO NPs-induced damage to biological systems, we established the exposure conditions for CuO NPs in subsequent experiments as 20 μg mL^{-1} for 12 h, based on the cytotoxicity outcomes.

3.2 CuO NPs are able to induce cuproptosis in RAW264.7 cells

RAW264.7 cells were exposed to varying concentrations of CuO NPs for a period of 12 h in order to further investigate the toxic mechanism of CuO NPs. The results showed a significant increase in intracellular copper levels (Fig. 2A), indicating that the accumulation of intracellular copper may be related to the toxicity induced by CuO NPs in RAW264.7 cells. Subsequently, an investigation into the relationship between cell impairment caused by CuO NPs and cuproptosis was conducted. The results revealed a significant, dose-dependent upregulation in the expression of critical genes associated with cuproptosis, such as dihydrolipoamide *S*-acetyltransferase (DLAT), LIAS, FDX1, and heat shock protein 70 (HSP70) (Fig. 2B). The lipoylation dihydrolipoamide *S*-acetyltransferase (Lip-DLAT) protein

4092 | *Environ. Sci.: Nano*, 2024, **11**, 4089–4101

This journal is © The Royal Society of Chemistry 2024

Fig. 1 Characterization of physical properties and cytotoxicity of CuO NPs. TEM characterization of the morphological features of 200 nm CuO NPs, scale bar, 200 nm (A), as well as the diameter analysis with Nano Measurer (B). The particle size (C) and the surface zeta potential (D) in different dispersing media with Malvern Zetasizer Nano ZEN3700. RAW264.7 cells were exposed to 20 $\mu g\ mL^{-1}$ CuO NPs for 0, 3, 6, 12, and 24 hours, and additionally to 0, 5, 10, and 20 $\mu g\ mL^{-1}$ CuO NPs for 12 hours to assess the time-dependent (E) and concentration-dependent (F) cytotoxicity of CuO NPs. Data are presented as mean ± SD. *$P < 0.05$, **$P < 0.01$, ***$P < 0.001$ compared to control. ns indicates no significance.

exhibited oligomerization, with the aggregation phenomenon notably escalating with increasing concentrations of CuO NPs (Fig. 2C and S1A†). The Lip-DLAT protein serves as a pivotal enzyme in the transformation of pyruvate within the tricarboxylic acid (TCA) cycle, playing a crucial role in its metabolic processes.[27] The oligomerization of Lip-DLAT leads to a reduction in pyruvate dehydrogenase activity,[35] resulting in the accumulation of pyruvate within cells (Fig. 2D). This phenomenon was evident in RAW264.7 cells exposed to various concentrations of CuO NPs for 12 h, demonstrating a notable, concentration-dependent rise.

3.3 CuO NPs induce ferroptosis in RAW264.7 cells through the release of copper ions

In this experiment, RAW264.7 cells were exposed to varying concentrations of CuO NPs for 12 h to investigate the occurrence of ferroptosis. The results demonstrated that elevated levels of intracellular copper ions significantly promoted the mRNA expression of transferrin receptor (TFR), ferroprotein (FPN), and ferritin heavy chain (FTH) (Fig. 3A). However, GPX4, the pivotal factor in cellular redox balance, exhibited a concentration-dependent decrease in both mRNA (Fig. 3A) and protein levels (Fig. 3B) in response to copper ions. The levels of MDA and LPO in RAW264.7 cells, key indicators of ferroptosis, also significantly increased with higher concentrations of CuO NPs (Fig. 3C, S2A and B†). Additionally, 100 μM TTM, the copper ion chelator, was employed to pretreat RAW264.7 cells for further investigation.

The results revealed a marked enhancement in cell viability following TTM pretreatment (Fig. 3D), which may be due to the inhibition of cuproptosis by intracellular copper ions.[23] Therefore, further characterization of the ferroptosis phenomenon remains necessary. Subsequent experiments indicated that the chelation of intracellular copper ions by TTM suppressed the expression of FTH and GPX4 at the mRNA level (Fig. 3E). At the protein level, the TTM pretreatment group exhibited a significant elevation in intracellular GPX4 content compared to the group treated solely with 20 $\mu g\ mL^{-1}$ CuO NPs (Fig. 3F). Moreover, intracellular LPO and MDA levels were notably diminished in the presence of TTM (Fig. 3G, S2C and D†).

3.4 Cuproptosis triggers ferroptosis by inhibiting mitochondrial membrane lipid synthesis

The disruption of intracellular redox homeostasis and iron homeostasis imbalance are the key mechanisms leading to ferroptosis.[31] Consequently, we conducted further investigations into the effects of CuO NPs exposure on intracellular redox homeostasis and iron content. Our findings showed that with the increase in CuO NPs concentration, there was no significant change in intracellular iron content (Fig. S3A†). However, the concentration-dependent decrease in GSH content (Fig. 4A) and the concentration-dependent increase in ROS levels (Fig. 4B) were observed. Mitochondrial damage is the primary factor leading to the disruption of intracellular redox homeostasis.[31,36] Consequently, we exposed RAW264.7 cells to varying

This journal is © The Royal Society of Chemistry 2024

Environ. Sci.: Nano, 2024, **11**, 4089–4101 | **4093**

Fig. 2 CuO NPs are able to induce cuproptosis in RAW264.7 cells. RAW264.7 cells were exposed to varying concentrations of CuO NPs (0, 5, 10, 20 μg mL^{-1}) for 12 h. (A) Following the harvesting and digestion of RAW264.7 cells, the intracellular copper content was quantified with inductively coupled plasma optical emission spectroscopy (ICP-OES). (B) The mRNA expression levels of DLAT, LIAS, FDX1, and HSP70 in RAW264.7 cells. (C) The expression and oligomerization status of Lip-DLAT protein in RAW264.7 cells. (D) Intracellular pyruvic acid levels. Data are presented as mean ± SD. **$P < 0.01$, ***$P < 0.001$ compared to control. ns indicates no significance.

concentrations of CuO NPs for 12 h, with or without TTM treatment, to evaluate mitochondrial impairment. Our findings revealed a pronounced escalation in mitochondrial damage with increasing concentrations of CuO NPs, which could be mitigated by TTM intervention (Fig. 4C).

Mitochondrial damage promotes an increase in intracellular ROS levels.[13,36,37] To further confirm whether ROS acts as the link between ferroptosis and cuproptosis, RAW264.7 cells were co-incubated at 37 °C for 1 h with 10 mM NAC, broad-spectrum ROS scavenger, 10 μM erastin, GSH depletion, and 10 μM Mito-TEMPO, mitochondria-targeted ROS scavenger, followed by exposure to 20 μg mL^{-1} CuO NPs for 12 h. Cell viability assays revealed a significant enhancement in cell viability in the NAC and Mito-TEMPO treatment groups, whereas the erastin treatment group exhibited a significant decrease in cell viability (Fig. 4D). Furthermore, experiments assessing intracellular GSH and ROS levels revealed a noteworthy elevation in GSH and a

decline in ROS levels with NAC and Mito-TEMPO treatment, while erastin treatment resulted in a significant reduction in GSH and an increase in ROS levels (Fig. S3B and C†). It has been reported that elevated intracellular ROS levels can trigger ferroptosis.[31] RAW264.7 cells exhibited a significant reduction in LPO under NAC and Mito-TEMPO treatment, while LPO was markedly enhanced under erastin treatment (Fig. 4E and S3D†). Correspondingly, both the mRNA and protein levels of GPX4 in RAW264.7 cells significantly increased with NAC and Mito-TEMPO treatment but decreased under erastin treatment (Fig. 4F, S4A and B†). In contrast, the experimental findings revealed that pretreatment with NAC, Mito-TEMPO, and erastin did not induce alterations in the mRNA expression of DLAT and FDX1 in RAW264.7 cells compared to the group exposed to 20 μg mL^{-1} CuO NPs (Fig. 4G and H). Additionally, no significant oligomerization of Lip-DLAT was observed (Fig. S4A and B†), and there was no significant variance in PA levels (Fig. S3E†).
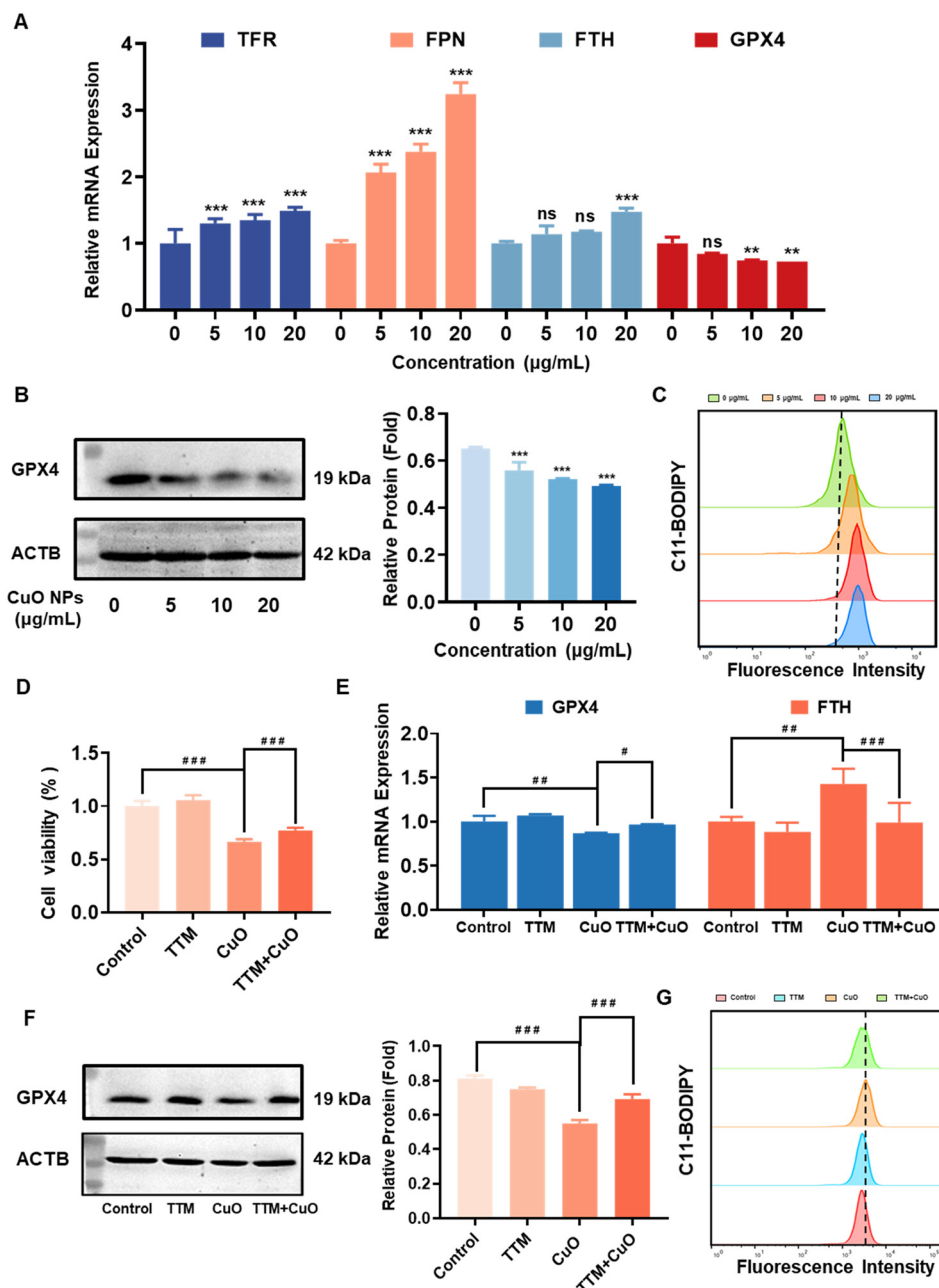
Fig. 3 CuO induces ferroptosis in RAW264.7 cells. RAW264.7 cells were exposed to different concentrations of CuO NPs (0, 5, 10, 20 μg mL^{-1}) for 12 h. (A) The levels of TFR, FPN, FTH, and GPX4 mRNA expression in RAW264.7 cells. (B) Expression and quantification of GPX4 protein in RAW264.7 cells. (C) Flow cytometry was employed to assess intracellular lipid peroxidation in RAW264.7 cells following staining with the fluorescent probe C11-BODIPY. RAW264.7 cells were pre-incubated with 100 μM TTM at 37 °C for 1 h, then exposed to 20 μg mL^{-1} CuO NPs for 12 h. (D) Cell viability post-treatment was assessed with CCK8 assay. (E) The alterations in GPX4 and FTH mRNA expression levels in RAW264.7 cells. (F) The detection of GPX4 protein expression. (G) Intracellular lipid peroxidation in RAW264.7 cells was evaluated by flow cytometry after staining with the fluorescent probe C11-BODIPY. Data are presented as mean ± SD. **$P < 0.01$, ***$P < 0.001$ compared to control. $^{\#}P < 0.05$, $^{\#\#}P < 0.01$, $^{\#\#\#}P < 0.001$ compared to 20 μg mL^{-1} CuO. ns indicates no significance.

Moreover, when compared to the group treated with 20 μg mL^{-1} CuO NPs, the NAC and Mito-TEMPO pretreatment group demonstrated aggravated mitochondrial impairment, whereas the erastin group displayed no notable alteration (Fig. S4C†).

Due to the multiple sources of intracellular ROS,[38] we conducted further investigations to confirm whether mitochondrial ROS is the predominant source of intracellular ROS. RAW264.7 cells were treated with varying concentrations

of CuO NPs for 12 h in the presence or absence of NAC and Mito-TEMPO. The findings revealed a significant increase in mitochondrial ROS levels with escalating CuO NPs concentrations, which was effectively attenuated by Mito-TEMPO and NAC treatments (Fig. 4I).

The reduction in pyruvate dehydrogenase activity resulting from cuproptosis disrupts the TCA cycle, impacting the synthesis and degradation of various cellular substances.[27]
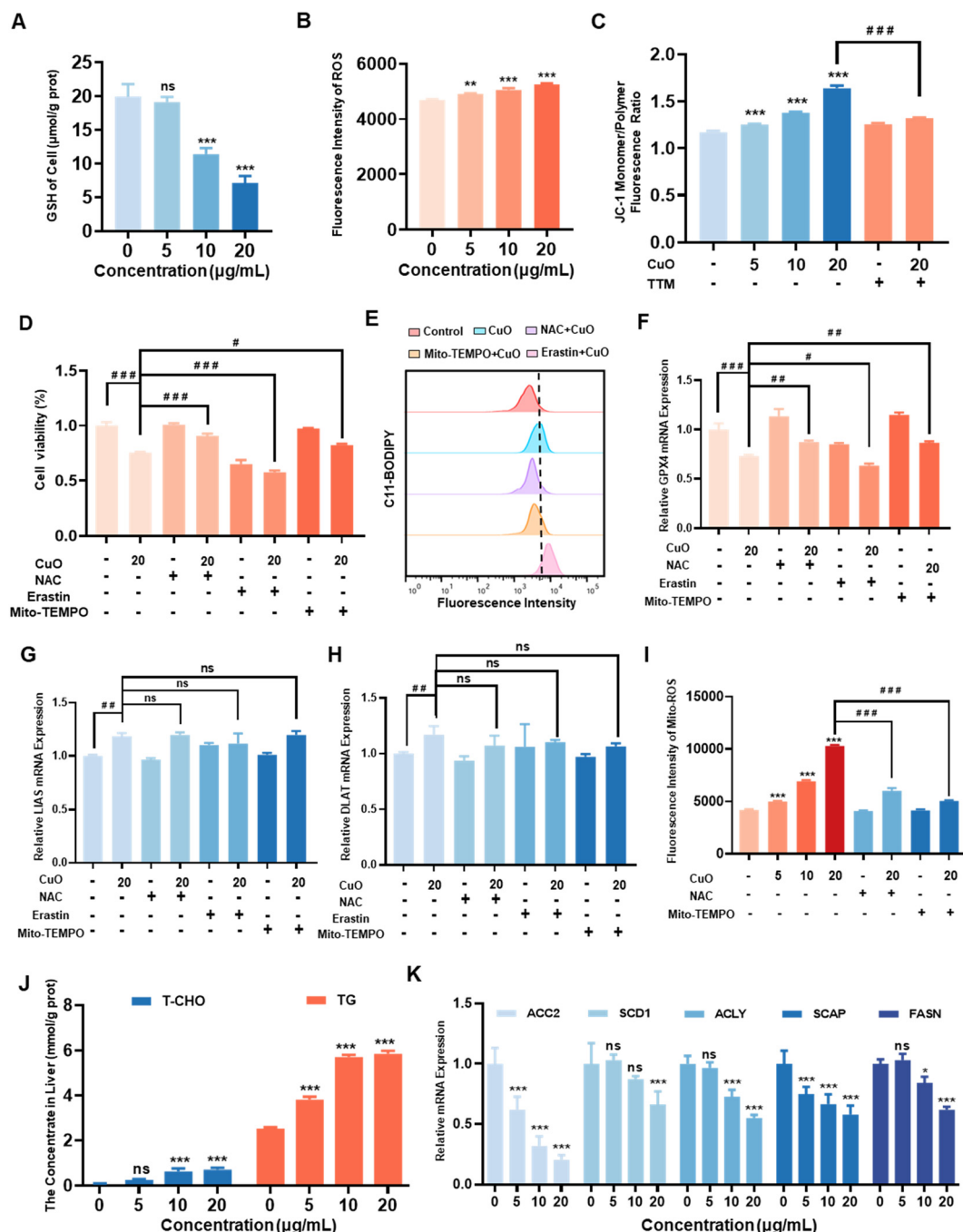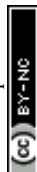
This journal is © The Royal Society of Chemistry 2024

Environ. Sci.: Nano, 2024, **11**, 4089–4101 | **4095**

Fig. 4 Cuproptosis triggers ferroptosis by inhibiting mitochondrial membrane lipid synthesis. RAW264.7 cells were exposed to different concentrations of CuO NPs for 12 h at 37 °C. The intracellular GSH content was measured (A), and intracellular ROS levels were detected using DCFH-DA fluorescence probe with flow cytometry (B). Additionally, RAW264.7 cells were exposed to different concentrations of CuO NPs for 12 h with or without pretreatment of 100 μM TTM, and the mitochondrial membrane potential was assessed using JC-1 mitochondrial membrane potential assay kit (C). Subsequently, RAW264.7 cells were co-incubated at 37 °C with 10 mM NAC, 10 μM erastin, and 10 μM Mito-TEMPO for 1 h, followed by exposure to 20 μg mL^{-1} CuO NPs for 12 h for analysis, including cell viability (D), intracellular lipid peroxidation using C11-BODIPY fluorescence probe staining (E), and mRNA expression levels of GPX4 (F), FDX1 (G), and DLAT (H). Moreover, RAW264.7 cells were co-incubated at 37 °C with 10 mM NAC and 10 μM Mito-TEMPO for 1 h, and then exposed to 20 μg mL^{-1} CuO NPs for 12 h to detect mitochondrial ROS levels using Mito-SOX red mitochondrial superoxide indicator (I). RAW264.7 cells were subjected to varying concentrations of CuO NPs for 12 h. The intracellular levels of T-CHO and TG (J), as well as the mRNA expression levels of ACC2, SCD1, ACLY, SCAP, and FASN, were also measured under these conditions (K). Data are presented as mean ± SD. **$P < 0.01$, ***$P < 0.001$ compared to control. $^{\#}P < 0.05$, $^{\#\#}P < 0.01$, $^{\#\#\#}P < 0.001$ compared to 20 μg mL^{-1} CuO. ns indicates no significance.

4096 | *Environ. Sci.: Nano*, 2024, **11**, 4089–4101

This journal is © The Royal Society of Chemistry 2024

Furthermore, the inhibition of mitochondrial membrane lipid synthesis leads to mitochondrial impairment and subsequently triggers ferroptosis.[39] Subsequent to RAW264.7 cell exposure to varying concentrations of CuO NPs for 12 h, there was a significant increase in intracellular T-CHO and

TG levels (Fig. 4J). The mRNA levels of proteins related to lipid synthesis, such as acetyl-CoA carboxylase (ACC2), stearoyl-CoA desaturase (SCD1), ATP citrate lyase (ACLY), SREBP cleavage-activating protein (SCAP), and fatty acid synthase (FASN),[39–44] displayed a noteworthy concentration-

Fig. 5 CuO leads to liver damage through mechanisms involving cuproptosis and ferroptosis. Male C57BL/6 mice, aged 6–8 weeks, were orally administered with doses of 0, 10, and 100 mg kg^{-1} of CuO NPs for 35 days. (A) The liver samples were collected and subjected to digestion for the quantification of copper and iron levels using ICP-OES. (B) The concentrations of ALT and AST in the plasma. (C) Liver tissues underwent H&E staining for histological examination, scale bar, 50 μm. (D) Liver slices were co-incubated with the C11-BODIPY fluorescent probe for 10 min to observe and quantify phospholipid peroxidation within the liver. (E) The levels of acetoacetic acid in the liver were determined. Scale bar, 100 μm. (F) The mRNA expression levels of FPN, TFR, FTH, GPX4, and FDX1 in the liver were evaluated. (G and H) Liver slices were also co-incubated with DCFH-DA and JC-1 fluorescent probes for 10 min to assess (G) ROS levels and (H) mitochondrial membrane potential, scale bar, 100 μm. Data are presented as mean ± SD. *$P < 0.05$, **$P < 0.01$, ***$P < 0.001$ compared to control. ns indicates no significance.

This journal is © The Royal Society of Chemistry 2024

Environ. Sci.: Nano, 2024, 11, 4089–4101 | 4097

dependent decrease (Fig. 4K). Furthermore, a significant decrease in intracellular ATP content was observed only in the highest dose group of 20 μg mL^{-1} (Fig. S4D†).

3.5 CuO NPs lead to liver damage through cuproptosis and ferroptosis

To further explore the potential involvement of cuproptosis and ferroptosis in the tissue damage induced by CuO NPs, we administered oral suspensions of 200 nm CuO NPs at doses of 10 and 100 mg kg^{-1} to mice for 35 days. The findings demonstrated significant copper accumulation in the liver, lungs, and brain tissues, mainly showing a concentration-dependent increase in accumulation within the liver (Fig. S5A†). Given the liver's pivotal role as the primary metabolic organ responsible for copper ion metabolism,[30] it was chosen for detailed investigation. Subsequent analysis revealed a significant accumulation of both copper and iron in the liver (Fig. 5A). Markedly reduced levels of ALT and AST in both blood and liver were observed (Fig. 5B and S5B†). The examination of mRNA expression levels of inflammatory factors in the liver unveiled a significant decrease in IL-10, accompanied by a significant increase in IL-6 and TNF-α (Fig. S5C†). Moreover, the findings from H&E staining indicated substantial liver damage (Fig. 5C).

Subsequently, we delved into the mechanisms underlying liver damage induced by CuO NPs. Our findings revealed a significant increasing trend in hepatic LPO (Fig. 5D) and a noticeable accumulation of PA (Fig. 5E). Further exploration indicated a significant upregulation in the mRNA expression levels of FTH, TFR, and FDX1, while GPX4 exhibited a significant decrease, and FPN showed no significant alteration in the liver (Fig. 5F). Additionally, a reduction in GPX4 protein expression and oligomerization of Lip-DLAT protein were observed in the liver (Fig. S5D†). Moreover, a significant increase in MDA content was observed (Fig. S5E†), while the levels of GSH and SOD significantly decreased (Fig. S5F and S6A†) in the liver. The fluorescent probe analysis of liver tissue slices revealed a significant increase in ROS levels (Fig. 5G) and exacerbated mitochondrial damage (Fig. 5H). Simultaneously, a significant decrease was observed in blood T-CHO and TG levels (Fig. S6B†), while TG levels in the liver remained unchanged, however, T-CHO exhibited a significant reduction in the highest concentration group (Fig. S6C†).

4. Discussion

Previous research has indicated that CuO NPs primarily inflict cellular damage through CuO particles and copper ions.[45–47] Research on the mechanism of copper ion-induced cellular damage has mainly focused on the Fenton reaction initiated by Cu ions interacting with intracellular components to generate ROS, as well as the consequences of elevated intracellular ROS levels on cells.[29,48–51] Recent studies have proposed that intracellular copper overload not only triggers the Fenton reaction but also induces the oligomerization of key proteins in the TCA cycle and the loss of Fe–S cluster proteins, ultimately

leading to cuproptosis.[23] Therefore, we selected CuO NPs to investigate the impact of cuproptosis on the biocompatibility of CuO NPs, while also delving into the mechanistic link between cuproptosis and other cell death by CuO NPs. The result supports the opinion that CuO NPs induce cuproptosis in RAW264.7 cells, with the manifestation of cuproptosis significantly increasing with escalating concentrations of CuO NPs, which may be due to the fact that once internalized by cells, CuO NPs are captured by lysosomes, triggering the release of copper ions and causing intracellular copper overload,[46,47] which is a prerequisite for cuproptosis.[23] Additionally, previous research indicated that ligands present in culture media can facilitate the release of copper ions from CuO NPs,[52] which could also be a contributing factor to the intracellular copper ion overload induced by CuO NPs.

Copper, as an essential trace element within cells, plays a pivotal role in various biochemical pathways crucial for maintaining cellular balance.[29,50] Research indicates that copper participates in the synthesis of the intracellular FTH protein.[30] Therefore, we hypothesized that CuO NPs might regulate ferroptosis. Our findings demonstrated the induction of ferroptosis in RAW264.7 cells by CuO NPs. Interestingly, detailed investigations into ferroptosis in RAW264.7 cells revealed an upregulation of intracellular FTH expression, leading to a decrease in free iron levels and the inhibition of ferroptosis.[31] Conversely, the decreased expression of GPX4 disrupted cellular redox balance, promoting ferroptosis.[31,34] Since the oxidative properties of CuO NPs, it remains uncertain whether the disturbance of intracellular redox homeostasis is stems from CuO particles themselves or the liberation of copper ions captured by lysosomes from CuO NPs. Therefore, TTM, a copper ion chelator, was used to further exploration. By integrating the experimental outcomes, we concluded that while CuO NPs can adjust free and bound iron levels within cells by modulating FTH synthesis to delay ferroptosis, the disruption of cellular redox balance by CuO NPs is more likely to instigate ferroptosis in RAW264.7 cells, a process dependent on the presence of copper ions in the form of CuO NPs.

CuO NPs triggered cuproptosis and ferroptosis in RAW264.7 cells, prompting our interest in exploring a potential connection between cuproptosis and ferroptosis. Notably, as we evaluated the intracellular redox balance, we observed an increase in ROS levels, raising the question of whether ROS could act as a signaling molecule between cuproptosis and ferroptosis. Previous research has indicated that the generation of ROS induced by CuO NPs is not linked to cuproptosis but rather occurs through the Fenton reaction, disrupting the intracellular redox equilibrium.[15,53] While this observation suggests that cuproptosis and ferroptosis are distinct phenomena without a direct relationship, we also observed that higher concentrations of CuO NPs led to intensified mitochondrial damage, with mitochondria playing a critical role in cuproptosis and ferroptosis.[23,37,54] Moreover, mitochondrial ROS emerged as a key source of intracellular ROS,[36] leading us to hypothesize that mitochondria may serve as a bridge between cuproptosis and ferroptosis.

4098 | *Environ. Sci.: Nano*, 2024, **11**, 4089–4101

This journal is © The Royal Society of Chemistry 2024

Subsequent experiments involving the use of NAC, Mito-TEMPO, and erastin on RAW264.7 cells revealed that changes in ROS levels selectively influenced ferroptosis while leaving cuproptosis unaffected. Furthermore, the worsening of mitochondrial damage due to decreased intracellular ROS levels but the alleviation of such damage by TTM indicated that not only the Fenton reaction but also cuproptosis-induced mitochondrial damage was responsible for the elevated intracellular ROS levels. Therefore, we propose that CuO NPs trigger cuproptosis in RAW264.7 cells, leading to mitochondrial damage, disruption of intracellular redox balance, and ultimately facilitating ferroptosis. Nonetheless, the exact mechanism by which cuproptosis impacts mitochondria remains to be elucidated.

Cuproptosis triggers the aggregation of Lip-DLAT protein, resulting in reduced pyruvate dehydrogenase complex activity and the inhibition of the TCA cycle.[27] The compromised TCA cycle disrupts the balance of various intracellular substances.[36] Simultaneously, research has shown that the decrease in pyruvate dehydrogenase complex activity leads to a reduction in acetyl-CoA levels, hindering fatty acid synthesis and initiating ferroptosis.[55,56] Elevated intracellular levels of T-CHO and TG indicate disturbances in lipid balance, accompanied by a notable decline in the expression of genes responsible for synthesizing lipids in the mitochondrial membrane, such as ACC2, SCD1, ACLY, SCAP, and FASN.[39] These combined findings imply that cuproptosis provokes mitochondrial damage and triggers ferroptosis by suppressing the gene expression of proteins essential for mitochondrial lipid synthesis and impeding fatty acid production. Notably, cuproptosis doesn't obstruct ATP synthesis.[23] Nevertheless, during the evaluation of mitochondrial damage, a significant reduction in ATP levels was observed at the highest concentration of CuO NPs, possibly due to copper ion-induced mitochondrial damage through the Fenton reaction.[48,49]

The liver serves as the primary organ responsible for metabolizing copper ions.[57] After the oral ingestion of CuO NPs, there is a notable accumulation of copper and iron ions in the liver, primarily due to the mutual regulatory interplay between copper and iron.[30] Findings from H&E staining and PCR analysis both reveal clear evidence of liver damage, coinciding with the occurrence of cuproptosis and ferroptosis. Subsequent investigations unveiled a reduction in hepatic lipid synthesis, mitochondrial dysfunction, and disturbance of the redox homeostasis, aligning with the results observed *in vitro* experiments.

5. Conclusion

In summary, following internalization by RAW264.7 cells, CuO NPs induce cuproptosis, which will suppress the expression of proteins essential for mitochondrial membrane lipid synthesis and impede fatty acid production to result in mitochondrial impairment. This disruption subsequently disrupts the intracellular redox balance, ultimately triggering ferroptosis. *In vivo*, experimental findings demonstrate that

CuO NPs induce liver damage through pathways involving cuproptosis and ferroptosis. These results offer additional insights into understanding cuproptosis and the safety implications of CuO NPs. However, the experimental findings merely establish a mechanistic link between cuproptosis and ferroptosis at a macroscopic level, failing to elucidate the precise molecular mechanisms and signaling pathways implicated. Furthermore, additional research is needed to explore the interplay between cuproptosis and other forms of cell death.

Data availability

The data supporting this article have been included as part of the ESI.†

Conflicts of interest

The authors declare that they have no known competing financial interests or personal relationships that could have appeared to influence the work reported in this paper.

Acknowledgements

References

1 R. Augustine, A. P. Mathew and A. Sosnik, Metal Oxide Nanoparticles as Versatile Therapeutic Agents Modulating Cell Signaling Pathways: Linking Nanotechnology with Molecular Medicine, *Appl. Mater. Today*, 2017, **7**, 91–103.

2 D. Maity, U. Gupta and S. Saha, Biosynthesized metal oxide nanoparticles for sustainable agriculture: next-generation nanotechnology for crop production, protection and management, *Nanoscale*, 2022, **14**(38), 13950–13989.

3 L. Y. Zhu, L. X. Ou, L. W. Mao, X. Y. Wu, Y. P. Liu and H. L. Lu, Advances in Noble Metal-Decorated Metal Oxide Nanomaterials for Chemiresistive Gas Sensors: Overview, *Nano-Micro Lett.*, 2023, **15**(1), 89.

4 M. Mesgari, A. H. Aalami, T. Sathyapalan and A. Sahebkar, A Comprehensive Review of the Development of Carbohydrate Macromolecules and Copper Oxide Nanocomposite Films in Food Nanopackaging, *Bioinorg. Chem. Appl.*, 2022, **2022**, 7557825.

5 X. Zhang, L. Detering, D. Sultan, H. Luehmann, L. Li and G. S. Heo, *et al.*, CC Chemokine Receptor 2-Targeting Copper Nanoparticles for Positron Emission Tomography-Guided Delivery of Gemcitabine for Pancreatic Ductal Adenocarcinoma, *ACS Nano*, 2021, **15**(1), 1186–1198.

6 S. I. Concha-Guerrero, E. M. S. Brito, H. A. Piñón-Castillo, S. H. Tarango-Rivero, C. A. Caretta and A. Luna-Velasco,

This journal is © The Royal Society of Chemistry 2024

Environ. Sci.: Nano, 2024, **11**, 4089–4101 | **4099**

et al., Effect of CuO Nanoparticles over Isolated Bacterial Strains from Agricultural Soil, *J. Nanomater.*, 2014, **2014**, 148743.

7 Q. B. Zhang, K. L. Zhang, D. G. Xu, G. C. Yang, H. Huang and F. D. Nie, *et al.*, CuO nanostructures: Synthesis, characterization, growth mechanisms, fundamental properties, and applications, *Prog. Mater. Sci.*, 2014, **60**, 208–337.

8 A. A. Keller and A. Lazareva, Predicted Releases of Engineered Nanomaterials: From Global to Regional to Local, *Environ. Sci. Technol. Lett.*, 2014, **1**(1), 65–70.

9 V. Rajput, T. Minkina, S. Sushkova, A. Behal, A. Maksimov and E. Blicharska, *et al.*, ZnO and CuO nanoparticles: a threat to soil organisms, plants, and human health, *Environ. Geochem. Health*, 2020, **42**(1), 147–158.

10 A. A. Keller, A. S. Adeleye, J. R. Conway, K. L. Garner, L. J. Zhao and G. N. Cherr, *et al.*, Comparative environmental fate and toxicity of copper nanomaterials, *NanoImpact*, 2017, **7**, 28–40.

11 S. Areecheewakul, A. Adamcakova-Dodd, Z. R. Zacharias, X. Jing, D. K. Meyerholz and K. L. Legge, *et al.*, Immunomodulatory Effects of Subacute Inhalation Exposure to Copper Oxide Nanoparticles in House Dust Mite-Induced Asthma, *ACS Nano*, 2023, **17**(15), 14586–14603.

12 Z. Su, C. Yao, J. Tipper, L. Yang, X. Xu and X. Chen, *et al.*, Nanostrategy of Targeting at Embryonic Trophoblast Cells Using CuO Nanoparticles for Female Contraception, *ACS Nano*, 2023, **17**(24), 25185–25204.

13 T. E. Henson, J. Navratilova, A. H. Tennant, K. D. Bradham, K. R. Rogers and M. F. Hughes, In vitro intestinal toxicity of copper oxide nanoparticles in rat and human cell models, *Nanotoxicology*, 2019, **13**(6), 795–811.

14 X. Wang, C. H. Chang, J. Jiang, X. Liu, J. Li and Q. Liu, *et al.*, Mechanistic Differences in Cell Death Responses to Metal-Based Engineered Nanomaterials in Kupffer Cells and Hepatocytes, *Small*, 2020, **16**(21), e2000528.

15 S. Naz, A. Gul, M. Zia and R. Javed, Synthesis, biomedical applications, and toxicity of CuO nanoparticles, *Appl. Microbiol. Biotechnol.*, 2023, **107**(4), 1039–1061.

16 G. Gupta, F. Cappellini, L. Farcal, R. Gornati, G. Bernardini and B. Fadeel, Copper oxide nanoparticles trigger macrophage cell death with misfolding of Cu/Zn superoxide dismutase 1 (SOD1), *Part. Fibre Toxicol.*, 2022, **19**(1), 33.

17 X. Lu, X. Chen, C. Lin, Y. Yi, S. Zhao and B. Zhu, *et al.*, Elesclomol Loaded Copper Oxide Nanoplatform Triggers Cuproptosis to Enhance Antitumor Immunotherapy, *Adv. Sci.*, 2024, **11**(18), e2309984.

18 K. H. Tsui, J. H. Hsiao, L. T. Lin, Y. L. Tsang, A. N. Shao and C. H. Kuo, *et al.*, The Cross-Communication of Cuproptosis and Regulated Cell Death in Human Pathophysiology, *Int. J. Biol. Sci.*, 2024, **20**(1), 218–230.

19 A. Gallo, L. Manfra, R. Boni, A. Rotini, L. Migliore and E. Tosti, Cytotoxicity and genotoxicity of CuO nanoparticles in sea urchin spermatozoa through oxidative stress, *Environ. Int.*, 2018, **118**, 325–333.

20 L. A. Jaragh-Alhadad and M. Falahati, Copper oxide nanoparticles promote amyloid-beta-triggered neurotoxicity through formation of oligomeric species as a prelude to

Alzheimer's diseases, *Int. J. Biol. Macromol.*, 2022, **207**, 121–129.

21 B. E. El Bialy, R. A. Hamouda, M. A. Abd Eldaim, S. S. El Ballal, H. S. Heikal and H. K. Khalifa, *et al.*, Comparative Toxicological Effects of Biologically and Chemically Synthesized Copper Oxide Nanoparticles on Mice, *Int. J. Nanomed.*, 2020, **15**, 3827–3842.

22 S. Chortarea, G. Gupta, L. A. Saarimaki, W. Netkueakul, P. Manser and L. Aengenheister, *et al.*, Transcriptomic profiling reveals differential cellular response to copper oxide nanoparticles and polystyrene nanoplastics in perfused human placenta, *Environ. Int.*, 2023, **177**, 108015.

23 P. Tsvetkov, S. Coy, B. Petrova, M. Dreishpoon, A. Verma and M. Abdusamad, *et al.*, Copper induces cell death by targeting lipoylated TCA cycle proteins, *Science*, 2022, **375**(6586), 1254–1261.

24 Y. Zhu, X. Niu, C. Ding, Y. Lin, W. Fang and L. Yan, *et al.*, Carrier-Free Self-Assembly Nano-Sonosensitizers for Sonodynamic-Amplified Cuproptosis-Ferroptosis in Glioblastoma Therapy, *Adv. Sci.*, 2024, e2402516.

25 C. L. Hao, L. Huang, H. Y. Zhang, L. G. Xu, M. Z. Sun and H. Kuang, *et al.*, Chiral CuxOS@Fe-MOFs for Enhanced Cancer Therapy, *Adv. Funct. Mater.*, 2024, **34**(10), 2312795.

26 Y. Li, J. Liu, Y. Chen, R. R. Weichselbaum and W. Lin, Nanoparticles Synergize Ferroptosis and Cuproptosis to Potentiate Cancer Immunotherapy, *Adv. Sci.*, 2024, e2310309.

27 M. A. Kahlson and S. J. Dixon, Copper-induced cell death, *Science*, 2022, **375**(6586), 1231–1232.

28 M. C. Linder, N. R. Zerounian, M. Moriya and R. Malpe, Iron and copper homeostasis and intestinal absorption using the Caco2 cell model, *BioMetals*, 2003, **16**(1), 145–160.

29 L. Chen, J. Min and F. Wang, Copper homeostasis and cuproptosis in health and disease, *Signal Transduction Targeted Ther.*, 2022, **7**(1), 378.

30 S. Gulec and J. F. Collins, Molecular mediators governing iron-copper interactions, *Annu. Rev. Nutr.*, 2014, **34**, 95–116.

31 M. Aschner, A. V. Skalny, A. C. Martins, A. I. Sinitskii, M. Farina and R. Lu, *et al.*, Ferroptosis as a mechanism of non-ferrous metal toxicity, *Arch. Toxicol.*, 2022, **96**(9), 2391–2417.

32 P. Zhang, C. Zhou, X. Ren, Q. Jing, Y. Gao and C. Yang, *et al.*, Inhibiting the compensatory elevation of xCT collaborates with disulfiram/copper-induced GSH consumption for cascade ferroptosis and cuproptosis, *Redox Biol.*, 2024, **69**, 103007.

33 W. K. Wang, K. Z. Lu, X. Jiang, Q. Wei, L. Y. Zhu and X. Wang, *et al.*, Ferroptosis inducers enhanced cuproptosis induced by copper ionophores in primary liver cancer, *J. Exp. Clin. Cancer Res.*, 2023, **42**(1), 142.

34 Q. Xue, D. Yan, X. Chen, X. Li, R. Kang and D. J. Klionsky, *et al.*, Copper-dependent autophagic degradation of GPX4 drives ferroptosis, *Autophagy*, 2023, **19**(7), 1982–1996.

35 R. A. Mathias, T. M. Greco, A. Oberstein, H. G. Budayeva, R. Chakrabarti and E. A. Rowland, *et al.*, Sirtuin 4 is a lipoamidase regulating pyruvate dehydrogenase complex activity, *Cell*, 2014, **159**(7), 1615–1625.

4100 | *Environ. Sci.: Nano*, 2024, **11**, 4089–4101

This journal is © The Royal Society of Chemistry 2024

36 J. B. Spinelli and M. C. Haigis, The multifaceted contributions of mitochondria to cellular metabolism, *Nat. Cell Biol.*, 2018, **20**(7), 745–754.

37 S. J. Oh, M. Ikeda, T. Ide, K. Y. Hur and M. S. Lee, Mitochondrial event as an ultimate step in ferroptosis, *Cell Death Discovery*, 2022, **8**(1), 414.

38 B. Niemann, S. Rohrbach, M. R. Miller, D. E. Newby, V. Fuster and J. C. Kovacic, Oxidative Stress and Cardiovascular Risk: Obesity, Diabetes, Smoking, and Pollution: Part 3 of a 3-Part Series, *J. Am. Coll. Cardiol.*, 2017, **70**(2), 230–251.

39 X. Yang, C. Gu, J. Cai, F. Li, X. He and L. Luo, *et al.*, Excessive SOX8 reprograms energy and iron metabolism to prime hepatocellular carcinoma for ferroptosis, *Redox Biol.*, 2024, **69**, 103002.

40 H. M. O'Neill, J. S. Lally, S. Galic, M. Thomas, P. D. Azizi and M. D. Fullerton, *et al.*, AMPK phosphorylation of ACC2 is required for skeletal muscle fatty acid oxidation and insulin sensitivity in mice, *Diabetologia*, 2014, **57**(8), 1693–1702.

41 J. Yi, J. Zhu, J. Wu, C. B. Thompson and X. Jiang, Oncogenic activation of PI3K-AKT-mTOR signaling suppresses ferroptosis via SREBP-mediated lipogenesis, *Proc. Natl. Acad. Sci. U. S. A.*, 2020, **117**(49), 31189–31197.

42 F. J. Dufort, M. R. Gumina, N. L. Ta, Y. Tao, S. A. Heyse and D. A. Scott, *et al.*, Glucose-dependent de novo lipogenesis in B lymphocytes: a requirement for atp-citrate lyase in lipopolysaccharide-induced differentiation, *J. Biol. Chem.*, 2014, **289**(10), 7011–7024.

43 T. F. Osborne and P. J. Espenshade, Lipid balance must be just right to prevent development of severe liver damage, *J. Clin. Invest.*, 2022, **132**(11), e160326.

44 H. Shin, S. Park, J. Hong, A. R. Baek, J. Lee and D. J. Kim, *et al.*, Overexpression of fatty acid synthase attenuates bleomycin induced lung fibrosis by restoring mitochondrial dysfunction in mice, *Sci. Rep.*, 2023, **13**(1), 9044.

45 N. Hanagata, F. Zhuang, S. Connolly, J. Li, N. Ogawa and M. Xu, Molecular responses of human lung epithelial cells to the toxicity of copper oxide nanoparticles inferred from whole genome expression analysis, *ACS Nano*, 2011, **5**(12), 9326–9338.

46 J. Zhang, Z. Zou, B. Wang, G. Xu, Q. Wu and Y. Zhang, *et al.*, Lysosomal deposition of copper oxide nanoparticles triggers HUVEC cells death, *Biomaterials*, 2018, **161**, 228–239.

47 H. L. Karlsson, P. Cronholm, J. Gustafsson and L. Möller, Copper oxide nanoparticles are highly toxic: A comparison between metal oxide nanoparticles and carbon nanotubes, *Chem. Res. Toxicol.*, 2008, **21**(9), 1726–1732.

48 K. Jomova and M. Valko, Advances in metal-induced oxidative stress and human disease, *Toxicology*, 2011, **283**(2–3), 65–87.

49 M. Valko, H. Morris and M. T. Cronin, Metals, toxicity and oxidative stress, *Curr. Med. Chem.*, 2005, **12**(10), 1161–1208.

50 Q. Xue, R. Kang, D. J. Klionsky, D. Tang, J. Liu and X. Chen, Copper metabolism in cell death and autophagy, *Autophagy*, 2023, **19**(8), 2175–2195.

51 K. Jomova, M. Makova, S. Y. Alomar, S. H. Alwasel, E. Nepovimova and K. Kuca, *et al.*, Essential metals in health and disease, *Chem.-Biol. Interact.*, 2022, **367**, 110173.

52 Z. Wang, A. von dem Bussche, P. K. Kabadi, A. B. Kane and R. H. Hurt, Biological and environmental transformations of copper-based nanomaterials, *ACS Nano*, 2013, **7**(10), 8715–8727.

53 H. He, Z. Zou, B. Wang, G. Xu, C. Chen and X. Qin, *et al.*, Copper Oxide Nanoparticles Induce Oxidative DNA Damage and Cell Death via Copper Ion-Mediated P38 MAPK Activation in Vascular Endothelial Cells, *Int. J. Nanomed.*, 2020, **15**, 3291–3302.

54 Z. Tian, S. Jiang, J. Zhou and W. Zhang, Copper homeostasis and cuproptosis in mitochondria, *Life Sci.*, 2023, **334**, 122223.

55 X. Song, J. Liu, F. Kuang, X. Chen, H. J. Zeh 3rd and R. Kang, *et al.*, PDK4 dictates metabolic resistance to ferroptosis by suppressing pyruvate oxidation and fatty acid synthesis, *Cell Rep.*, 2021, **34**(8), 108767.

56 C. Li, X. Dong, W. Du, X. Shi, K. Chen and W. Zhang, *et al.*, LKB1-AMPK axis negatively regulates ferroptosis by inhibiting fatty acid synthesis, *Signal Transduction Targeted Ther.*, 2020, **5**(1), 187.

57 M. M. Pena, J. Lee and D. J. Thiele, A delicate balance: homeostatic control of copper uptake and distribution, *J. Nutr.*, 1999, **129**(7), 1251–1260.

This journal is © The Royal Society of Chemistry 2024

Environ. Sci.: Nano, 2024, **11**, 4089–4101 | **4101**